



## **AIAA 98-3770**

### **Flame-Vortex Interactions in a Non-Premixed H<sub>2</sub>/N<sub>2</sub>/Air Counterflow Burner**

G. J. Fiechtner, C. D. Carter and K. D. Grinstead, Jr.  
Innovative Scientific Solutions, Inc.  
Dayton, OH

J. R. Gord and W. M. Roquemore  
Air Force Research Laboratory  
Wright-Patterson AFB, OH

J. C. Rolon  
École Centrale Paris  
Paris, France

**34th AIAA/ASME/SAE/ASEE  
Joint Propulsion Conference & Exhibit  
July 13-15, 1998 / Cleveland, OH**

# FLAME-VORTEX INTERACTIONS IN A NON-PREMIXED H<sub>2</sub>/N<sub>2</sub>/AIR COUNTER-FLOW BURNER

Gregory J. Fiechtner,<sup>1,4,5</sup> Campbell D. Carter,<sup>1,4</sup> James R. Gord,<sup>2,4</sup>  
Keith D. Grinstead, Jr.,<sup>1</sup> W. M. Roquemore,<sup>2,4</sup> and J. C. Rolon<sup>3</sup>

## **Abstract**

The dynamic interaction between a laminar flame and a vortex is examined. The hydroxyl (OH) layer produced by the flame is imaged using planar laser-induced fluorescence (PLIF), and preliminary vortex-characterization data are acquired using acetone PLIF and digital, two-color particle-image velocimetry (PIV). The PIV and PLIF measurements of OH are performed simultaneously. The hydrogen-air flame is supported in a nonpremixed opposed-jet burner. The apparatus is found to produce highly repeatable events, making it ideal for studying the interaction between a flame and an isolated vortex. A distinct annular extinction of the OH layer is observed, in good agreement with previous computational modeling predictions of the apparatus.

## **Introduction**

Recent results in numerical modeling combined with experimental measurements have led to important advances in the understanding of combustion. Numerous investigations have contributed to these advances, including a particular type of study in which the inter-

action between a laminar, nonpremixed flame and a vortex is examined. These efforts involve repeatable, carefully controlled conditions that are highly amenable to experimental study.

In recent computational calculations, Katta<sup>1</sup> predicted that during the interaction of a nonpremixed hydrogen-air flame and an isolated vortex, the extinction of the OH layer would occur in an annular pattern. The experiments detailed in this paper are performed to examine, in part, the validity of this prediction. Experimental results obtained with planar laser-induced fluorescence (PLIF) of OH are used to determine regimes in which the annular, Katta-type extinction occurs. The nonpremixed flame is supported by air and fuel in an opposed-jet burner. The fuel consists of hydrogen diluted with nitrogen. The amount of hydrogen in nitrogen is varied, along with the strength of the vortex. The temporal evolution of flame-vortex interactions is imaged with the PLIF system.

Additional measurements were performed to characterize vortices. First, acetone was seeded into the vortex and its laser-excited fluorescence is detected. Second, particles were seeded into the flowfield and the scattering was used for digital, two-color particle-image velocimetry (PIV) measurements. Digital PIV measurements are made simultaneously with PLIF measurements of OH. Preliminary vortex-characterization results are discussed in this paper.

## **Background**

Numerous experimental studies of the interaction dynamics of vortices and flames have been conducted, and many of these investigations employed two-dimensional imaging to study the interaction. For premixed flame fronts, most measurements have been made using two types of flames. Hertzberg et al.<sup>2</sup> and Escudie<sup>3</sup> conducted an experiment in which a Karman vortex street was produced using a cylindrical rod in a cross flow of premixed gases. A V-flame was supported behind a wire positioned downstream of the rod that produced the vortex street. Planar tomographic imaging was used to study the interaction of the vortex street with the flame. A similar interaction between a

<sup>1</sup>Innovative Scientific Solutions, Inc., 2766 Indian Ripple Road, Dayton, OH 45440-3638, USA.

<sup>2</sup>Propulsion Directorate, Air Force Research Laboratory, Wright-Patterson Air Force Base, OH 45433-7103, USA.

<sup>3</sup>Laboratoire d'Énergétique Moléculaire et Macroscopique, Combustion, École Centrale Paris, Grande Voie des Vignes, 92295 Châtenay-Malabry Cedex, France.

<sup>4</sup>Member, AIAA.

<sup>5</sup>Corresponding author and presenter.

This paper is declared a work of the U.S. Government and is not subject to copyright protection in the United States.

Karman vortex street and a flame was investigated by Lee et al.<sup>4</sup> using PLIF imaging of OH and by Nye et al.<sup>5</sup> using both OH PLIF and PIV. A disadvantage of using the vortex street is the difficulty in isolating a single vortex. Nguyen and Paul<sup>6</sup> studied a more isolated interaction by replacing the Karman vortex street with a line vortex pair directed into one side of a V-flame. The vortex-injection process was found to be highly repeatable.

In a second type of study involving premixed combustion, Jarosinski et al.<sup>7</sup> studied a flame that was ignited at one end of a tube of premixed gases. A vortex was injected at the other end of the tube. The interaction dynamics were then photographed using a mercury-xenon arc lamp and a rotating-drum streak camera with a rotating-disc shutter. Recently, Driscoll and co-workers produced an impressive series of papers concerning a similar flame-vortex apparatus in which PIV, OH PLIF, or a combination of these imaging techniques was applied.<sup>8-18</sup>

Nonpremixed flames have also been the subject of experimental study. Rolon and co-workers<sup>19-21</sup> recently developed an apparatus in which a vortex is injected into a flame supported between the nozzles of an opposed-jet burner. This geometry has numerous advantages. First, unlike the above geometries, a stationary nonpremixed flame can easily be produced and isolated. Second, the flame thickness can be varied by changing either the nozzle velocities or the spacing between the upper and lower burner nozzles. The apparatus has also been extended to the study of vortices that interact with premixed opposed-jet flames.<sup>22</sup>

In a different class of measurements, Hsu et al.<sup>23</sup> modulated the axial velocity of a laminar jet diffusion flame using a loud speaker to produce flame-vortex interactions. The same apparatus was further studied by Hancock and coworkers<sup>24-28</sup> using a number of techniques including reactive Mie scattering, PLIF, and digital PIV. The studies have successfully provided extensive quantities of data for comparison with numerical modeling predictions. A disadvantage is the complicated geometry when compared to those geometries above due to the convective velocity field associated with rotation of the vortex and translation of the flame zone.<sup>24</sup> In addition, the angle of incidence between the vortex and the flame differs from that in experiments above and also from that in some turbulent combustion conceptualizations.<sup>29</sup>

More recently, Chen and Dahm<sup>30</sup> developed a facility for generating a nonpremixed burning layer that wraps into a vortex ring. The facility allows experiments to be performed under conditions of both normal gravity and microgravity, thereby removing the influence of buoyancy from the results.

The experiments described in this paper are based on the counterflow geometry of Rolon and co-workers,

and the observations described below rely heavily on the progress outlined in their papers.<sup>19-22</sup> A fuel mixture of hydrogen and nitrogen permits the use of laser diagnostics in the absence of hydrocarbon interferences, and the reaction zone of these nonpremixed flames is generally much thicker than that for premixed flames. The comparatively simple hydrogen-chemistry mechanisms simplify the numerical calculations that are the subject of comparison with experimental results.

## **Apparatus and Procedure**

### **Burner Facility**

A picture (a) and diagram (b) of the burner are shown in Figure 1. The configuration is based on the design of Rolon et al.<sup>19-22</sup> The flame is supported between upper and lower nozzles separated by 40 mm, each with an exit diameter of 25 mm. The fuel consists of hydrogen diluted with nitrogen and flows from the upper nozzle. Air flows from the lower nozzle. Unique to this type of apparatus is a tube with 5-mm inner diameter that is installed concentrically within the lower nozzle. This tube is attached to a cylinder that contains a piston, which in turn is attached to an actuator. Feeding an appropriate current to the actuator causes a solenoid to force the piston upward abruptly, resulting in the emergence of a vortex from the tube. The vortex travels upward within the surrounding oxidizer flow. A flow of air is supplied to the vortex tube such that, in the absence of a vortex, the exit velocity matches the velocity of the air from the surrounding nozzle. To minimize the impact of room-air disturbances, upper and lower guard flows of nitrogen are supported through outer nozzles, which are concentric with the respective upper and lower inner nozzles that support the flame.

The hydrogen, nitrogen diluent, and oxidizer air flows are furnished by mass-flow controllers with full-scale ranges of 20 l/min, 20 l/min, and 30 l/min, respectively. A continuous flow of air is provided to the vortex tube by a 5-l/min controller, while the guard flow from the upper and lower guard (outer) nozzles is furnished by two 50-l/min mass flow controllers. The flow rates of each controller are accurate to  $\pm 1\%$  of the full-scale range. The experiments have been repeated for several different flame conditions, as summarized in Table I.

The vortex properties can be varied by changing the magnitude and the rise time of the current that is fed to the actuator. The impedance of the actuator ranges from 1  $\Omega$  to 1.5  $\Omega$ , depending on the frequency content of the current. At full displacement, a current of up to 6 A is provided to the solenoid by a specially designed, high-speed power amplifier. This can result in consid-

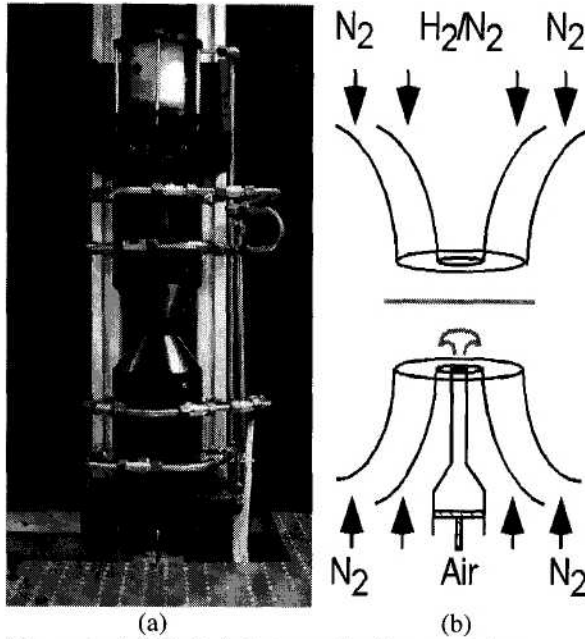


Figure 1: (a) Digital photograph of opposed-jet burner. (b) Cross-sectional diagram of burner nozzles and piston.

Table I: Flow rates (l/min) at 21.5°C and 724 mm Hg for five flame conditions.  $X_{H_2}$  is volume fraction of hydrogen in nitrogen diluent.

Gas	Flame					
	A	B	C	D	E	F
H <sub>2</sub>	2.76	3.40	4.04	4.67	5.31	5.94
N <sub>2</sub> Diluent	17.1	17.1	17.1	17.0	17.0	16.9
$X_{H_2}$	0.14	0.17	0.19	0.22	0.24	0.26
Air	11.2	11.2	11.2	11.2	11.2	11.2

erable power consumption by the actuator if the full-displacement condition is maintained for long periods. Consequently, an AC waveform is supplied by initial application of a negative potential, causing the piston to be withdrawn from the flame. The negative potential is applied for about 0.5 s to allow the flame to recover from this initial disturbance, as verified by digital, two-color PIV. The potential is then quickly changed to a positive value of the same magnitude with a carefully controlled rise time,  $\tau_r$ . The strength of the vortex can be increased by increasing the current magnitude, which results in a larger displaced-fluid volume through the exit of the tube. Eventually, the maximum displacement of the solenoid is reached. In this case, the vortex strength can be further increased by using a smaller value of  $\tau_r$ . The relationship among volume displacement,  $\tau_r$ , and the vortex characteristics has been discussed in numerous papers, including those by Rolon et al.,<sup>19</sup> Roberts,<sup>9</sup> and Chen and Dahm.<sup>30</sup> The

drive current for the solenoid is obtained by power amplifying the output of a digital arbitrary-waveform generator. This generator is operated at its maximum number of 10,000 quantized steps, resulting in a minimum stepsize of 0.1 ms. For all measurements discussed in this paper,  $\tau_r$  is set at 10 ms.

Visualization of the vortex formation and propagation via acetone PLIF is accomplished using a vaporizer that is installed between the vortex tube and the mass-flow controller. A bypass valve allows adjustment of acetone seeding level. Because the acetone changes the flame characteristics, these visualization studies are limited to non-reacting flows. When the acetone studies are not required, the acetone vaporizer is removed from the apparatus.

Seed particles are introduced into the burner flows when digital PIV measurements of the vortex velocity are performed. Three particle seeders are installed: One seeder is placed after the oxidizer-air mass-flow controller and another after the vortex-air mass-flow controller. The third seeder is installed after the junction where the hydrogen and nitrogen gases are mixed. With the use of three seeders, each flow can be seeded with particles individually, or combinations of the different flowfields can be seeded. Each seeder contains hollow spherical ceramic particles with an approximate mean diameter of 2.4  $\mu\text{m}$ . When PIV studies are not required, the seeders are removed from the apparatus.

### Laser Diagnostics: OH PLIF Imaging

The PLIF system contains a frequency doubled, Q-switched Nd:YAG laser that is used to pump a dye laser which is, in turn, frequency doubled. The light is directed through a telescope that is adjusted to produce a light sheet with a height that matches as nearly as possible the 40-mm burner separation. The resulting beam thickness is  $\sim 300 \mu\text{m}$ , which corresponds to the full width at 25% peak of the intensity profile, and  $\sim 15 \text{ mJ/pulse}$  is available at the test section.

Hydroxyl radicals absorb the laser radiation at 281.3414 nm via the  $R_1(8)$  transition of the (1,0) band in the A-X system. Fluorescence from the A-X (1,1) and (0,0) bands is detected at right angles through WG-295 and UG-11 colored-glass filters, followed by a 105-mm focal length,  $f/4.5$  UV lens. The resulting light reaches an intensified CCD camera with an intensifier gate width of 100 ns. CCD pixels are binned in 2x2 groups. The magnification is set to obtain an image with 7,509 binned groups per meter, corresponding to an imaged area of 25.6 mm by 38.4 mm. The bottom of the image is 0.25-mm above the surface of the lower nozzle. A color table is used with a maximum value set to 95% of the maximum signal for all images taken at a given flame condition. The low-signal color is assigned

by calculating the background noise and selecting a minimum value that is two standard deviations above this level. Therefore, in cases in which “extinction” of the OH layer is observed, “extinction” refers to signal levels that fall below this minimum value and are, therefore, assigned the last color in the table. All images represent the signal collected during a single laser shot, and no smoothing of the resulting images is attempted.

In studies of flame-vortex interactions by other investigators,<sup>31</sup> LIF was applied as a marker of some other quantity such as heat release or burning rate. In the present experiments, the OH image is obtained for direct comparison with numerical computations of the OH distribution;<sup>1</sup> therefore, no attempt is made to correlate the images with any other quantities.

Acetone PLIF imaging is accomplished using the OH PLIF imaging system. Here, the UG-11 colored-glass filter is removed to permit collection of the acetone fluorescence.

### **Laser Diagnostics: Digital, Two-Color PIV**

Measurements of the velocity field are implemented using digital, two-color PIV.<sup>32,33</sup> Here, a color digital CCD<sup>34</sup> with an array of 3060 x 2036 pixels<sup>2</sup> is used. A magnification of 78,368 pixels/m is employed, resulting in an imaged area of 26.0 mm by 39.0 mm. The color CCD camera and the intensified CCD array are aligned using a transparent mask printed with a graduated scale. Further alignment between images is performed using software after each experiment, when a transformation in two-dimensional space is applied to the PIV images relative to the PLIF images. Two lasers are used, with one PIV sheet produced by directly doubling the output of a Q-switched Nd:YAG laser (30 mJ/pulse at the test section). The remainder of this beam is used to pump the dye laser that is frequency doubled to excite OH fluorescence. The second PIV light sheet is produced by pumping a dye laser (employing DCM laser dye) with a second frequency-doubled, Q-switched Nd:YAG laser, resulting in laser radiation at 640 nm (40 mJ/pulse at the test section). The thickness of both the red and green sheets is set to ~700  $\mu\text{m}$ . A digital delay generator is used to drive the timing of the two lasers such that the red pulses are delayed precisely with respect to the green pulses. In the absence of a vortex, the underlying counterflow velocity field is probed with red pulses that are delayed by up to 1 ms with respect to the corresponding green pulses. For the fastest vortices studied, the delay between red and green pulses is reduced to 10  $\mu\text{s}$ . The camera shutter is set to open for 1/15 s to permit both laser pulses to be detected by the color CCD. Most of the flame emission and light from other devices in the

laboratory (monitors, etc.) is greatly attenuated by the shutter.

Velocity vectors are calculated using the correlation software of Gogenini and co-workers.<sup>32</sup> A correlation area of 128 pixels by 128 pixels is used in the calculation, corresponding to a correlation area of 0.269  $\text{cm}^2$  and a spatial resolution of 1.6 mm. In these preliminary studies, the main interest in digital PIV measurements is to obtain the propagation velocity of the vortex, and this correlation area is acceptable for such a purpose. We have also obtained excellent results using correlation areas as small as 32 pixels x 32 pixels, which will be utilized in future studies in which quantities such as strain are calculated. Neighboring correlation boxes are overlapped by 75%, resulting in a velocity field with an area of 95 vectors by 60 vectors, or 5700 total vectors over the area of the color ccd. In some portions of each image, a small percentage of bad vectors results because of low seed levels, scattering of light into the camera, flame emission, and other effects. Because the flame-vortex interactions are repeatable, digital PIV images can be recorded until an image with an extremely small percentage of incorrect vectors is obtained. For this reason, nearly 15 gigabytes of digital color image data were acquired.

Characterization of vortices is illustrated in Figure 2, where a single, idealized vortex ring is drawn superimposed over an axisymmetric cylindrical coordinate system using the coordinates  $z$  and  $u$  to illustrate the forward position and velocity, respectively. The coordinates  $r$  and  $v$  represent the radial position and velocity, respectively. In this coordinate representation, the vorticity simplifies to

$$\vec{\zeta} = \Delta \times \vec{V} = \frac{\partial v}{\partial z} - \frac{\partial u}{\partial r}. \quad (1)$$

In these preliminary studies, evaluation of the derivatives in eq. (1) are carried out without smoothing of the velocity field. Because this can amplify noise, future calculations will be performed using an appropriate smoothing algorithm.<sup>35,36</sup> When the velocity field is the final desired result from reduction of digital PIV images, it is common to filter out bad vectors, resulting in “holes” in the field that must be filled using a variety of techniques such as interpolation.<sup>37</sup> However, the resulting interpolated holes will be a source of significant error in vorticity computations.<sup>35,36</sup> Therefore, images with more than a few bad vectors are discarded before attempting to compute vorticity. In the future, an optimum method of computing the velocity field will be implemented so that the uncertainty in vorticity results because of these holes can be reduced.<sup>35,36</sup> Before plotting images of vorticity, a 3x3 smoothing function that is provided with the commercially available Transform® software, is applied four times. In these preliminary studies, the resulting images are used

to study the relative distribution of vorticity as a vortex propagates upward from the lower nozzle. In future studies in which the influence of the flame on the vorticity is examined and quantitative vorticity information is then extracted, a more accurate method of computing and displaying the vorticity will be implemented.<sup>35,36</sup>

The vortex circulation is computed using the integral over the contour shown in Figure 2, yielding<sup>38,39</sup>

$$\Gamma = \oint_e \vec{V} \cdot d\vec{s} = \sum_i \sum_j \vec{V}_{ij} \cdot s_{ij} = \sum_i \sum_j \zeta_{ij} A_{\text{cell}} \quad (2)$$

where  $e$  represents a contour box whose sides are drawn along lines where the vorticity remains below approximately 10% of its peak value (found at the core). The line integral method (the first double summation) and the vorticity integral method (the second double summation) are found to agree within 20%. To confirm the choice of contour and the integration process, the integration is performed over each side of the vortex depicted in Figure 2, and the resulting sum is determined to approach zero.

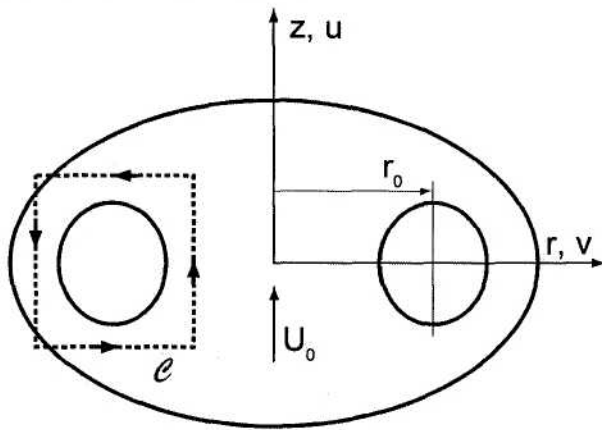


Figure 2. Coordinate system and integration contour used during computation of vortex properties.<sup>35,36,40</sup>

### **Synchronization and Timing**

Precise synchronization of several experimental events, including vortex generation and propagation, production of laser pulses, and activation of the camera shutter or intensifier, is required. A block diagram of the synchronization scheme is shown in Figure 3.

Because the Nd:YAG lasers are designed to operate at a nominal repetition rate of 10 Hz, the experimental sequence must be synchronized to a 10-Hz master clock that drives the flash lamps and the Pockels cells of the lasers. To trigger the laser(s), the clock sends two signals, one of which travels to a 50- $\Omega$  power combiner and then the laser digital delay generator (DDG). The 10-Hz clock also provides a TTL signal to

one of two inputs of a coincidence unit. The second input of the coincidence unit is driven by a TTL pulse from the PLIF camera controller. The coincidence unit outputs a pulse only when pulses from both the 10-Hz clock and the PLIF camera controller are present. When a flame-vortex event is initiated using a personal computer, the PLIF camera controller outputs a pulse approximately 1.3 s in duration. The corresponding output of the coincidence unit is a 1.3-s envelope of TTL pulses spaced by 100 ms. The first pulse in this envelope triggers a master DDG, synchronizing it with the 10-Hz clock and the laser pulse train. This DDG triggers an arbitrary-waveform generator (AWG) that outputs a 1-s waveform, which is amplified and fed to the piston actuator to generate a vortex. Approximately 0.5 s after the AWG waveform is initiated, the vortex is fired; therefore, five laser pulses are generated during the time between computer initiation and the flame-vortex interaction.

When the DDG is externally triggered, the jitter between the trigger and a DDG output pulse is 60 ps plus the output delay divided by  $10^8$ . Over the 0.5-s period between the first and fifth laser pulses, this corresponds to a jitter of 5.06 ns. The 10-Hz clock jitter specifications are not nearly so good. The jitter between clock outputs is 1 part in 10,000, corresponding to a jitter of 50  $\mu$ s over the same 0.5-s period. Attempting to synchronize the piston with the clock severely limits the temporal resolution available to "freeze" flame-vortex events in time and requires an intensifier gate width significantly larger than 50  $\mu$ s. The master DDG is therefore configured to trigger the fifth laser pulse preemptively. A delayed pulse from the master DDG arrives at the 50- $\Omega$  power combiner just before the fifth pulse in the clock pulse train, preemptively triggering the laser(s). If no initiation pulse is output from the computer, the laser(s) are triggered by the 10-Hz clock as usual. This approach reduces the jitter in the timing of the fifth laser pulse from 50  $\mu$ s to approximately 5 ns while maintaining the nominal 10-Hz repetition rate required by the lasers.

Other outputs of the master DDG are suitably delayed and directed to the image detectors. For PIV experiments, the width of a TTL pulse is adjusted using a gate generator, which closes a relay to trigger the digital PIV camera system. For simultaneous PLIF experiments, another master-DDG output triggers a pulse generator, which, in turn, activates the intensifier of an ICCD camera.

The scheme depicted in Figure 3 provides precise control of the relative timing between the laser diagnostics and the flame-vortex event. To explore the temporal evolution of the event, data are captured utilizing this phase-locked timing sequence: 1) an image is recorded, 2) the delay between vortex production and the laser/camera events is adjusted, and 3)

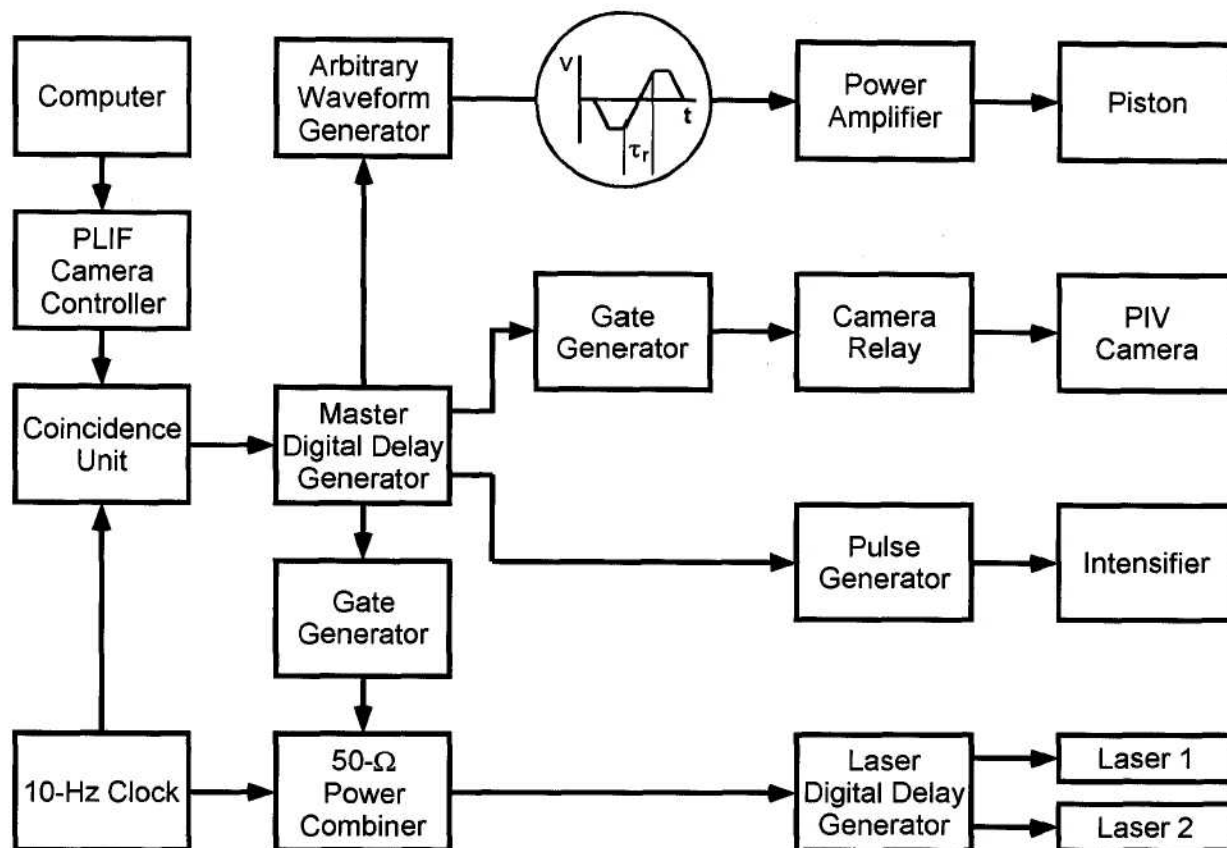


Figure 3: Diagram of electronic timing connections for simultaneous OH PLIF and digital PIV measurements.

another vortex is initiated and a second image is recorded. This process is repeated to acquire numerous images, each obtained at increasing delay, then an animation is created by assembling the individual images in temporal order. Effective temporal separation between images is selected between  $10\ \mu\text{s}$  and  $200\ \mu\text{s}$ , depending on the time scale of the event under study. The resulting animations are a testament to the high degree of repeatability achievable with this apparatus.

### Results and Discussion

#### Vortex Characterization

The sequence of acetone images in Figure 4 is typical of the sequential images used to measure the vortex-propagation velocity for a given amplitude and rise time of the solenoid drive current. The six images in the figure are selections from a sequence of fifty images, each delayed by  $100\ \mu\text{s}$  relative to the previous image. If the location of the flame front in the absence of a vortex is known, the acetone-PLIF image sequence can be used to estimate the velocity of the vortex at this location. In this case, the propagation velocity is  $\sim 5\ \text{m/s}$ .

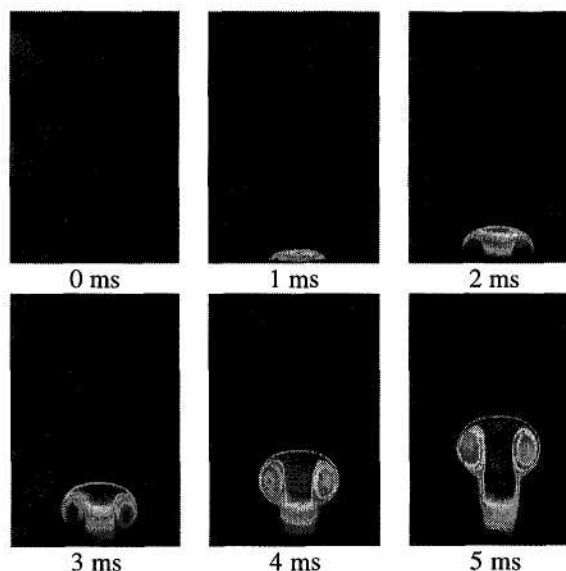


Figure 4: Acetone PLIF images of vortex.

Recently, characterization of vortex properties has been initiated using PIV, which is accomplished simultaneously with the OH PLIF measurements. Digital, two-color PIV measurements are readily made

when the flame is burning, offering a significant advantage over the acetone PLIF measurements of the vortex propagation velocity. Figure 5 contains the scattering signal obtained when seeding the vortex-tube flow with a slightly higher particle density than that produced by the upper- and lower-burner seed levels. The corresponding set of vectors is shown in Figure 6. The maximum vector length in the forward direction yields a propagation velocity of 0.77 m/s in this case.

Three different vortices are shown in Figure 7 by their respective vorticity fields, including a “weak,” an “intermediate,” and a “strong” vortex in columns (a), (b), and (c), respectively. The weak vortex has a circulation of approximately  $76 \text{ cm}^2/\text{s}$  and an initial propagation velocity of 1 m/s. However, the propagation velocity of this vortex slows to only 0.6 m/s by the fifth frame (labeled “50 ms”). Meanwhile, the distance between cores is  $2r_0=7 \text{ mm}$  in the first frame (labeled “0 ms”) and increases to nearly 15 mm in the fifth frame.

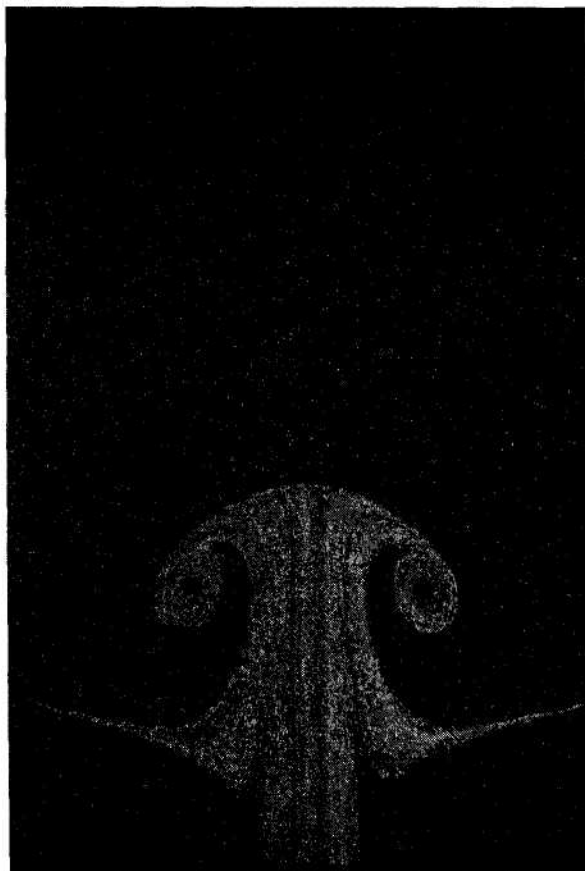


Figure 5: Scattering from particles in vortex flow.

In contrast, the intermediate vortex shown in the middle column of Figure 7 has a circulation of  $170 \text{ cm}^2/\text{s}$  and an initial propagation velocity of 2.2 m/s. By the time the vortex reaches the position shown in the fifth frame of column two, the propagation velocity has decreased to 1.8 m/s. The intermediate vortex shown in

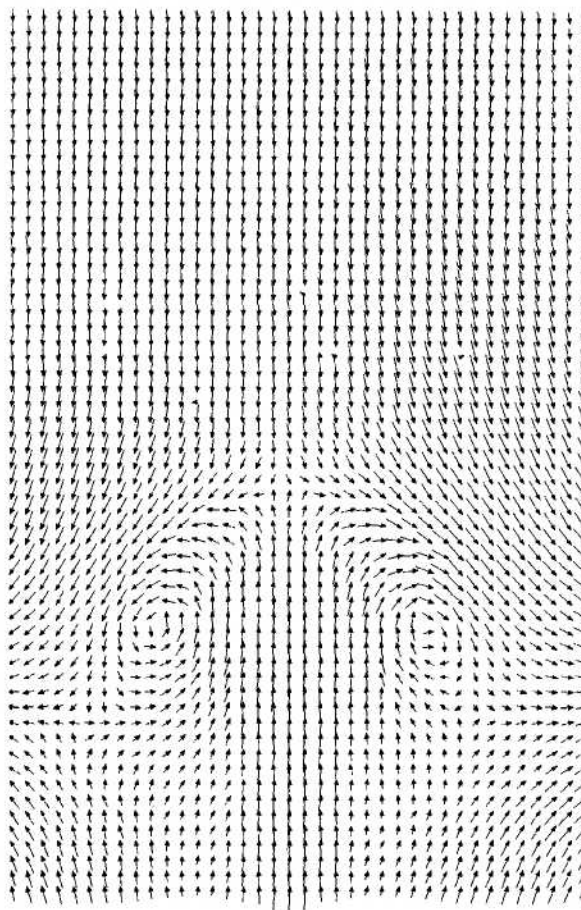


Figure 6: Vectors calculated from PIV image of Figure 5.

the first frame of column (b) has a distance between cores of approximately  $2r_0=7.8 \text{ mm}$ , which increases to  $\sim 12 \text{ mm}$  by the fifth frame of column two. The third column (c) contains the time-resolved vorticity field for a “strong” vortex, which has a circulation of  $1200 \text{ cm}^2/\text{s}$ . This vortex has a propagation velocity of 8.4 m/s in the first frame. The velocity increases to a value of 10 m/s in the fourth frame and then decreases to 9.5 m/s in the fifth frame of column (c). The strong vortex has a core separation of  $2r_0=8 \text{ mm}$  in the first frame, and the diameter grows to a value of  $\sim 10.5 \text{ mm}$  by the fifth frame of column (c). The strong vortex is observed to enter the upper-burner nozzle after the fifth frame. Care must be taken when attempting to generate a vortex that is stronger than case (c) as three-dimensional lobe structure can be possible.<sup>41</sup>

### Regimes of Flame-Vortex Interaction

The PLIF images of OH shown in Figure 8 correspond to a flame-vortex interaction in which extinction of the OH layer is absent. Initially, the vortex creates a small dent in the flame, and this dent then grows. Eventually the flame nearly surrounds the advancing

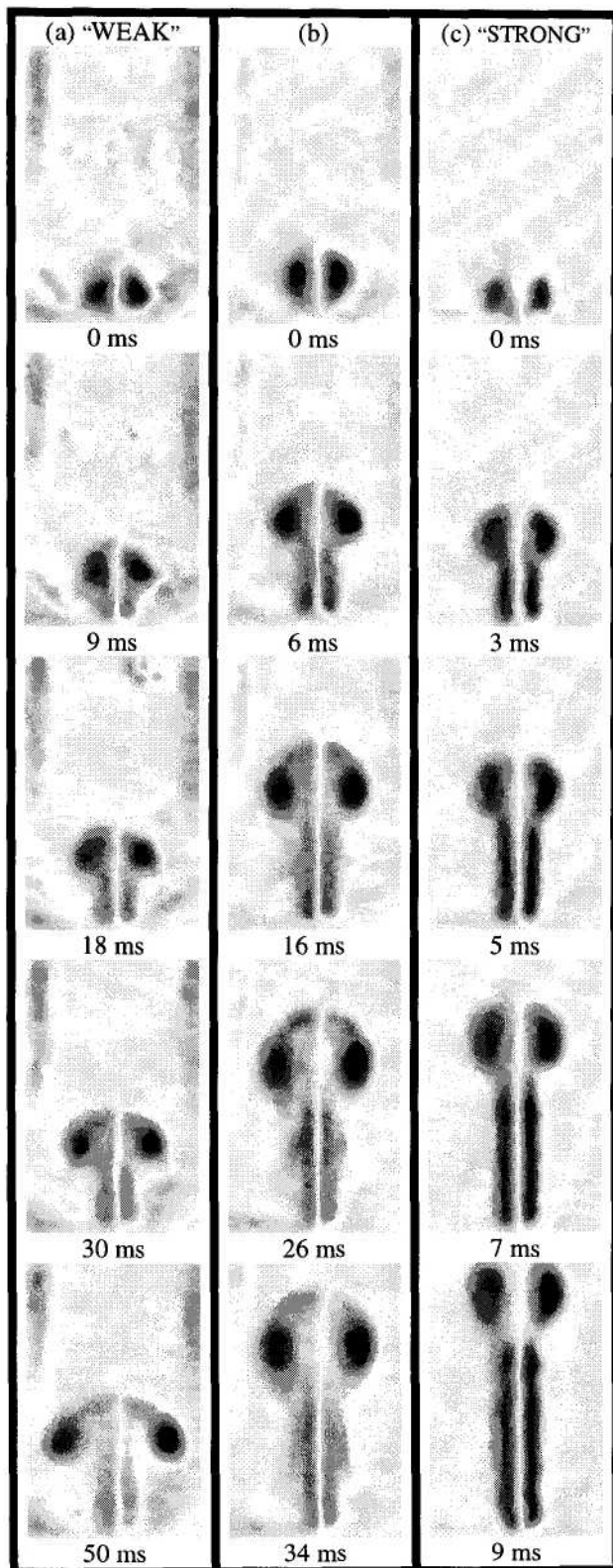


Fig. 7. Vorticity fields for three different vortices, each shown in a different column denoted by (a), (b), and (c).

vortex as it approaches the upper nozzle. In the later interaction stages, the OH PLIF signal level is observed to increase by greater than a factor of five over the levels observed without a vortex. The increased signal level is indicated by the light colors in the frames of Figure 8. This change in OH signal level is thought to indicate enhanced burning. For this particular example, the flow rates of Flame D in Table I are used.

The images of Figure 9 are obtained with flow conditions corresponding to Flame E in Table I and a vortex that is considered to be "strong". Extinction of the OH layer takes place in an annular pattern around the sides of the vortex, leaving a burning layer at its leading edge. This behavior was first predicted numerically by Katta,<sup>1</sup> well before these experiments were initiated, attesting to the utility of his code. After extinction, the isolated island of flame burns away, and the vortex travels upward toward the other nozzle. The flame follows the vortex, traveling up the stem. As the flame overtakes the vortex, it wraps up and turns in upon itself.

### Conclusions and Future Research

The apparatus of Rolon and co-workers<sup>19-22</sup> has been implemented to study of the interaction of a flame with a vortex. PLIF measurements of acetone and digital, two-color PIV have been applied to characterize the vortices injected into the opposed-jet flow. PLIF images of OH have been used to observe the dynamics of the interaction of the flame with the vortex. An annular break in the OH layer has been observed in excellent agreement with the numerical computations of Katta.<sup>1</sup>

Future work will be directed toward the understanding of phenomena such as the Katta-type extinction. A variety of parameters can be studied, such as extended ranges of nitrogen dilution in hydrogen, different flame-thickness regimes, and different fuels. To aid in these studies, simultaneous OH PLIF and digital, two-color PIV continue to be employed, along with measurements of the temperature field.

### Acknowledgements

The authors are grateful for the assistance and expert advice of Dr. J. M. Donbar regarding the two-color, digital PIV experiments and reduction of the resulting data. The authors wish to acknowledge the advice of Drs. L. P. Goss, S. Gogineni, and J. Estevadeordal concerning the reduction of two-color PIV data. The authors wish to thank Dr. R. D. Hancock and Illari Vihinen for assistance in assembly and construction of the burner. The authors also acknowledge Drs. J. M. Donbar, R. D. Hancock, W. M. Roquemore, V. R. Katta, and K.-Y. Hsu for the stimulating discussions of

flame-vortex dynamics. Finally, the authors wish to thank M. M. Whitaker for editing this manuscript. This work was supported by Air Force Contracts F33615-95-C-2507 and F33615-97-C-2702.

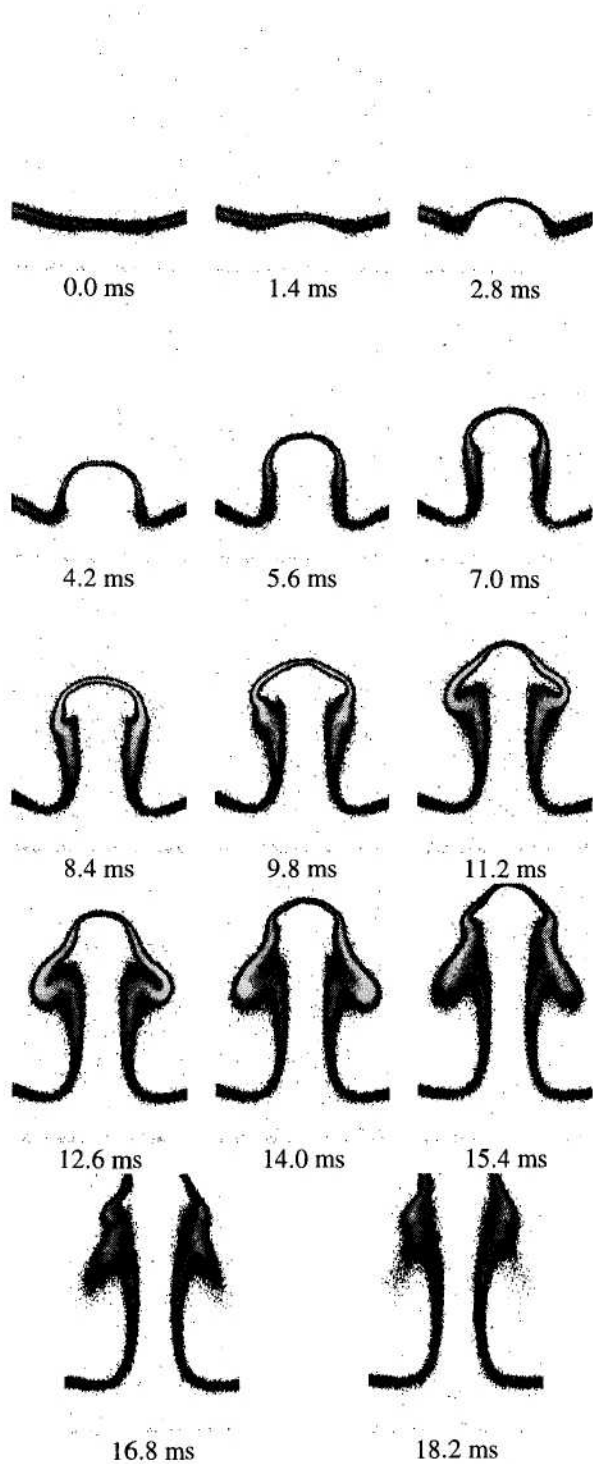


Fig. 8. OH PLIF images when OH layer remains intact.

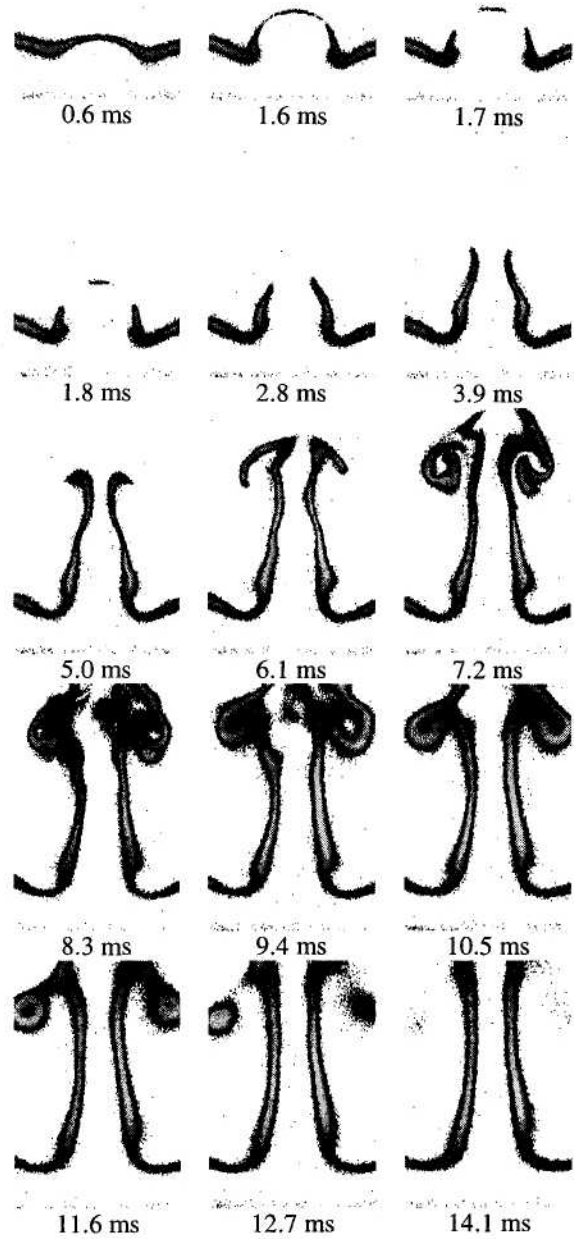


Figure 9: Sequence of images before and after extinction of the OH layer.

### References

1. V. R. Katta, C. D. Carter, G. J. Fiechtner, W. M. Roquemore, J. R. Gord, and J. C. Rolon, "Interaction of a Vortex With a Flat Flame Formed Between Opposing Jets of Hydrogen and Air," ac-

- cepted for publication in *Twenty-Seventh Symposium (International) on Combustion*, The Combustion Institute, Pittsburgh, 1998.
2. J. R. Hertzberg, M. Namazian, and L. Talbot, "A Laser Tomographic Study of a Laminar Flame in a Karman Vortex Street," *Combustion Science and Technology*, Vol. 38, No. 3/4, pp. 205-216, 1984.
  3. D. Escudie, "Stability of a Premixed Laminar V-Shaped Flame," *Progress in Astronautics and Aeronautics*, Vol. 113, pp. 215-239, 1988.
  4. T.-W. Lee, J. G. Lee, D. A. Nye, and C. A. Santavicca, "Local Response and Surface Properties of Premixed Flames During Interactions with Karman Vortex Streets," *Combustion and Flame*, Vol. 94, No. 1/2, pp. 146-160, 1993.
  5. D. A. Nye, J. G. Lee, T.-W. Lee, and D. A. Santavicca, "Flame Stretch Measurements During the Interaction of Premixed Flames and Karman Vortex Streets Using PIV," *Combustion and Flame*, Vol. 94, No. 1/2, pp. 167-176, 1996.
  6. Q.-V. Nguyen, and P. H. Paul, "The Time Evolution of a Flame-vortex Interaction Observed via Planar Imaging of CH and OH," *Twenty-Sixth Symposium (International) on Combustion*, The Combustion Institute, Pittsburgh, pp. 357-364, 1996.
  7. J. Jarosinski, J. H. S. Lee, and R. Knystautas, "Interaction of a Vortex Ring and a Laminar Flame," *Twenty-Second Symposium (International) on Combustion*, Pittsburgh, pp. 505-514, 1988.
  8. W. L. Roberts and J. F. Driscoll, "A Laminar Vortex Interacting with a Premixed Flame: Measured Formation of Pockets of Reactants," *Combustion and Flame*, Vol. 87, No. 3/4, pp. 245-256, 1991.
  9. W. L. Roberts, "A Premixed Laminar Flame Interacting With a Vortex Resulting in Flame Stretch and Quenching," Ph.D. Dissertation, University of Michigan, Ann Arbor, 1992.
  10. W. L. Roberts, J. F. Driscoll, M. C. Drake, and J. W. Ratcliffe, "OH Fluorescence Images of the Quenching of a Premixed Flame During an Interaction with a Vortex," *Twenty-Fourth Symposium (International) on Combustion*, The Combustion Institute, Pittsburgh, pp. 169-176, 1992.
  11. J. F. Driscoll, D. J. Sutkus, W. L. Roberts, M. E. Post, and L. P. Goss, "The Strain Exerted by a Vortex on a Flame – Determined from Velocity Field Images," AIAA Paper No. 93-0362.
  12. W. L. Roberts, J. F. Driscoll, M. C. Drake, and L. P. Goss, "Images of the Quenching of a Flame by a Vortex – To Quantify Regimes of Turbulent Combustion," *Combustion and Flame*, Vol. 94, No. 1/2, pp. 58-69, 1993.
  13. J. F. Driscoll, D. J. Sutkus, W. L. Roberts, M. E. Post, and L. P. Goss, "The Strain Exerted by a Vortex on a Flame – Determined from Velocity Field Images" *Combustion Science and Technology*, Vol. 4/6, pp. 213-229, 1994.
  14. C. J. Mueller, J. F. Driscoll, D. J. Sutkus, W. L. Roberts, M. C. Drake, and M. D. Smooke, "Effect of Unsteady Stretch Rate on OH Chemistry During a Flame-vortex Interaction: To Assess Flamelet Models," *Combustion and Flame*, Vol. 100, No. 1/2, pp. 323-331, 1995.
  15. C. J. Mueller, J. F. Driscoll, D. L. Ruess, and M. C. Drake, "Effects of Unsteady Stretch on the Strength of a Freely-Propagating Flame Wrinkled by a Vortex," *Twenty-Sixth Symposium (International) on Combustion*, The Combustion Institute, Pittsburgh, pp. 347-355, 1996.
  16. C. J. Mueller, "Measurements of Flame-vortex Interaction Dynamics and Chemistry," Ph.D. Dissertation, University of Michigan, Ann Arbor, 1996.
  17. J. O. Sinibald, C. J. Mueller, J. F. Driscoll, "Measured Local Propagation Velocities of Wrinkled Premixed Flames," Proceedings of the *Fall Technical Meeting*, The Eastern States Section of the Combustion Institute, Hartford, CT, pp. 179-182, 1997.
  18. C. J. Mueller, J. F. Driscoll, D. L. Ruess, M. C. Drake, and M. E. Rosalik, "Vorticity Generation and Attenuation as Vortices Convect Through a Premixed Flame," *Combustion and Flame*, Vol. 112, No. 3, pp. 342-358, 1998.
  19. J. C. Rolon, F. Aguerre, and S. Candel, "Experiments on the Interaction Between a Vortex and a Strained Diffusion Flame," *Combustion and Flame*, Vol. 100, No. 3, pp. 422-429, 1995.
  20. D. Thevenin, J. C. Rolon, P.-H. Renard, D. W. Kendrick, D. Veynante, and S. Candel, "Structure of a Nonpremixed Flame Interacting with Counter-rotating Vortices," *Twentieth-Sixth Symposium (International) on Combustion*, The Combustion Institute, Pittsburgh, pp. 1079-1086, 1996.
  21. D. Thevenin, P.-H. Renard, J. C. Rolon, and S. Candel, "Extinction Processes During a Non-Premixed Flame/Vortex Interaction," accepted for publication in *Twenty-Seventh Symposium (International) on Combustion*, The Combustion Institute, Pittsburgh, 1998.
  22. P.-H. Renard, J. C. Rolon, D. Thevenin, and S. Candel, "Wrinkling, Pocket Formation and Double Premixed Flame Interaction Processes," accepted for publication in *Twenty-Seventh Symposium (International) on Combustion*, The Combustion Institute, Pittsburgh, 1998.

23. K. Y. Hsu, L. D. Chen, V. R. Katta, L. P. Goss, and W. M. Roquemore, "Experimental and Numerical Investigations of the Flame-vortex Interactions in a Driven Jet Diffusion Flame," *31<sup>st</sup> Aerospace Sciences Meeting and Exhibit*, Reno, NV, January, 1993. AIAA Paper No. 93-0455.
24. R. D. Hancock, "Laser Diagnostic Investigation of the Structure of Steady and Driven Hydrogen Jet Diffusion Flames," Ph.D. Dissertation, University of Illinois, Urbana, 1996.
25. R. D. Hancock, F. R. Schauer, R. P. Lucht, V. R. Katta, and K. Y. Hsu, "Thermal Diffusion Effects and Flame-vortex Interactions in Hydrogen Jet Diffusion Flames," *Twenty-Sixth Symposium (International) on Combustion*, The Combustion Institute, Pittsburgh, pp. 1087-1093, 1996.
26. R. D. Hancock, F. R. Schauer, R. P. Lucht, and R. L. Farrow, "Dual-Pump Coherent Anti-Stokes Raman Scattering (CARS) Measurements of Nitrogen and Oxygen in a Laminar Jet Diffusion Flame," *Applied Optics*, Vol. 36, No. 15, pp. 3217-3226, 1997.
27. F. R. Schauer, "Thermal Diffusion and Flame Structure in a Laminar Hydrogen Jet Diffusion Flame," Ph.D. Thesis, University of Illinois, Urbana, 1998.
28. F. R. Schauer, R. D. Hancock, S. Gogineni, and R. P. Lucht, "Flame-vortex Interactions in Hydrogen Jet Diffusion Flames: A DPIV and DNS Investigation," submitted to *Experiments in Fluids*, 1998.
29. For example, see D. R. Ballal and A. H. Lefebvre, "The Structure and Propagation of Turbulent Flames," *Proc. R. Soc. London Ser. A*, Vol. 344, pp. 217-234, 1975.
30. S.-J. Chen and W. J. A. Dahm, "Vortex Ring/Diffusion Flame Interactions in Microgravity Conditions," Proceedings of the *Fourth International Microgravity Combustion Workshop*, Cleveland, OH, pp. 191-196, 1997. NASA Conference Publication No. 10191.
31. See, for example: H. N. Najm, P. H. Paul, C. J. Mueller, and P. S. Wyckoff, "On the Adequacy of Certain Experimental Observables as Measurements of Flame Burning Rate," *Combustion and Flame*, Vol. 113, No. 3, pp. 312-332, 1998.
32. S. Gogineni, L. Goss, D. Pestian, and R. Rivir, "Two-Color Digital PIV Employing a Single CCD Camera," *Experiments in Fluids*, in press, 1998.
33. J. M. Donbar, "Reaction Zone Structure and Velocity Measurements in Permanently Blue Non-premixed Jet Flames," Ph.D. Dissertation, University of Michigan, Ann Arbor, 1998.
34. R. P. Khosla, "From Photons to Bits," *Physics Today*, Vol. 45, No. 12, pp. 42-49, 1992.
35. J. D. Luff, A. M. Rompage, M. A. Linne, and J. R. Hertzberg, "Uncertainties Associated with the Post-Processing of 2-D Particle Image Velocimetry (PIV) Velocity Data of Unsteady Flow Fields," presented at the *Spring Meeting of the Western States Section of the Combustion Institute*, Tempe, AZ, March, 1996. Paper No. WSS 96S-005.
36. J. D. Luff, T. Drouillard, A. M. Rompage, M. A. Linne, and J. R. Hertzberg, "Experimental Uncertainties Associated with Particle Image Velocimetry (PIV) Based Vorticity Algorithms," to appear in *Experiments in Fluids*, Vol. 25, 1998.
37. S. Gogineni, L. Goss, and M. Roquemore, "Manipulation of a Jet in a Cross Flow," *Experimental Thermal and Fluid Science*, Vol. 16, pp. 209-219, 1998.
38. R. W. Fox and A. T. McDonald, "Introduction to Fluid Mechanics," John Wiley & Sons, New York, 1985.
39. J. W. Daily and D. R. F. Harleman, "Fluid Dynamics," Addison-Wesley Publishing, Reading, MA, 1966.
40. J. P. Sullivan, S. E. Widnall, and S. Ezekiel, "Study of Vortex Rings Using a Laser Doppler Velocimeter," *AIAA Journal*, Vol. 11, No. 10, pp. 1384-1389, 1973. Also presented at the *AIAA 11<sup>th</sup> Aerospace Sciences Meeting*, Washington, DC, January 1973. AIAA Paper No. 73-105.
41. S. E. Widnall, "The Structure and Dynamics of Vortex Filaments," *Annu. Rev. Fluid. Mech.*, Vol. 7, pp. 141-165, 1975.